

# Mechanism and Rate Law for High-Temperature Carboxylic Acid Corrosion of Steels

Ishan P. Patel, Gheorghe Bota, Peng Jin,<sup>†</sup> and David Young\*

Cite This: <https://doi.org/10.1021/acs.energyfuels.4c01284>

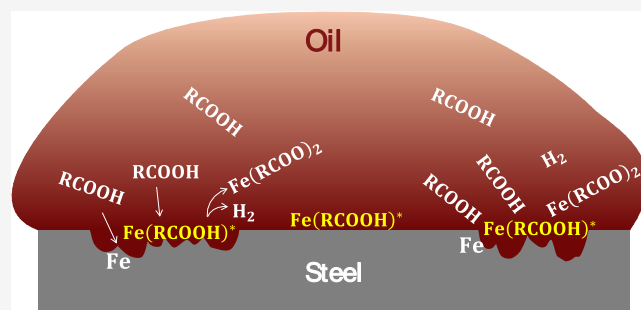
Read Online

ACCESS |

Metrics & More

Article Recommendations

**ABSTRACT:** High-temperature corrosion of steel by carboxylic acids in the oil phase, an oxidative dissolution process, is commonly encountered in refinery environments. Its reaction mechanism, as proposed herein, involves the formation of an active intermediate. The reaction rate law is obtained by applying a pseudo-steady-state hypothesis for the rate of formation of this active intermediate. Experimental corrosion rates of carbon steel versus concentrations of carboxylic acids closely fits ( $R^2 \approx 0.99$ ) with the derived rate law. Commonly observed first-order kinetics at higher concentrations of acids are discussed as a specific case of the derived rate law, advancing prior explanations of observed kinetics.



## INTRODUCTION

High-temperature nonaqueous corrosion of steel by carboxylic acids remains a predominant issue in oil refineries, especially for those choosing to process cheaper opportunity crudes with high acid content.<sup>1</sup> Oil prices are projected to remain high,<sup>2</sup> which compels refineries to process cheaper acidic crudes to sustain profitability.<sup>3</sup> Furthermore, refineries are also facing statutory requirements to coprocess a certain fraction of highly acidic bio-oils with conventional crude oils.<sup>4–9</sup> This raises concerns for the integrity of distillation units due to the highly unpredictable behavior of high-temperature carboxylic acid corrosion.<sup>10,11</sup> Under these circumstances, a reliable prediction of corrosion rates becomes crucial for high-stakes decisions. Therefore, an accurate mechanism of high temperature carboxylic acid corrosion is sought to model the kinetics of the carboxylic acid reaction with steel for the calculation of corrosion rates.

High-temperature corrosion of steel by carboxylic acids occurs between 220 and 400 °C by the following generalized redox reaction.<sup>12</sup>



Here, Fe represents carbon steel, and R is an aliphatic moiety. Naturally occurring organic acids in crude oils are popularly known as “naphthenic acids” due to cycloaliphatic moieties in their molecular structure.<sup>13</sup> However, they are simply referred to as carboxylic acids herein because aliphatic moieties in these acids consist of both acyclic and cyclic parts.<sup>14–17</sup> There is a vast variety of carboxylic acid structures in crude oils<sup>17</sup> and obviously their corrosivity varies. It may be postulated that the corrosion reaction mechanism essentially remains the same,

although at different rates, for organic acids in the oil phase since the products of corrosion remain the same. The acids are known to decompose by different mechanistic pathways.<sup>18–22</sup> Moreover, they also catalytically convert by metal and metal oxide surfaces to different compounds.<sup>23,24</sup> However, it can be hypothesized that the mechanistic pathway for the corrosion reaction A should remain the same if acids react with the metal for corrosion.

Carboxylic acid corrosion represented by reaction A can be described as an oxidative dissolution of iron by comparison with other organic metal leaching systems.<sup>25,26</sup> It can be inferred from the above reaction that the overall process essentially involves the movement of acid molecules in oil toward the steel surface followed by a redox reaction and ultimately the release of iron carboxylates.<sup>25</sup> Kinetics of these apparent mechanistic steps must be modeled to build a comprehensive prediction model for this corrosion phenomenon.

An attempt has been made to check whether the mechanism of high temperature carboxylic acid corrosion can be studied using electrochemical techniques, but it was instantly recognized that such measurements in the oil phase were deceptive in terms of faradaic conversion of applied current

Received: March 18, 2024

Revised: May 8, 2024

Accepted: May 16, 2024

into mass loss.<sup>1</sup> This confirmed that it is not possible to physically partition the nonelectrolytic redox reaction A into anodic and cathodic reactions by applying an external electric current. Further, any use of an electrolyte to enable electrochemical measurements would just force the reaction to follow an artificial electrochemical pathway, which would prove futile for investigating the actual high temperature reaction mechanism.

Some researchers have postulated that this reaction proceeds by the adsorption of carboxylic acids on the steel surface, resulting in its oxidation.<sup>27,28</sup> First of all, the use of the term “adsorption” can be misconstrued since the adsorption-based chemical reactions are presumably catalytic in which the substrate is not contained in the reaction. Second, a flattening of the corrosion rate would have been observed with an increase in the concentration of acids by saturating the metal surface, if any such adsorption-like step was involved. However, no such flattening of the corrosion rate has been observed; rather, the corrosion rate of carbon steel has been observed to increase monotonically as a function of acid concentration.<sup>1,19,26,27,29,30</sup> Thus, it is more appropriate to describe the noncatalytic interaction of carboxylic acids with iron as proceeding via an “active” intermediate, even if purely from a terminological perspective.<sup>31,32</sup> The corrosion rates of carbon and low alloy steels are known to depend linearly on the concentration of carboxylic acids for a given chemical composition of oil phase.<sup>1,19,26,27,29,30</sup> The linear relation between corrosion rate and concentration is often expressed on “log–log graph” to cover wide ranges of concentrations and related corrosion rates.<sup>1,19,27</sup> It is obvious from these data that the corrosion rates do not “flatten” for virtually any higher concentrations, refuting any adsorption mediated mechanisms involving surface saturation with an increasing concentration.

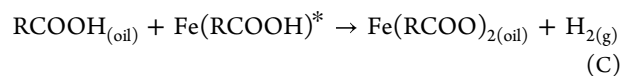
For the kinetic modeling of carboxylic acid corrosion, it is necessary to determine elementary reaction steps.<sup>33</sup> Hence, the mechanism of high temperature carboxylic acid corrosion is proposed herein by hypothesizing a sequence of elementary steps for reaction A to derive the reaction rate law, which validates kinetic measurements performed in this work and elsewhere. It is also anticipated that the proposed mechanism has general applicability to other organic-metal leaching systems.

## THEORY

**Mechanism.** As illustrated by reaction A, two carboxylic acid molecules react with iron to form iron carboxylate typically in the temperature range from 220 to 400 °C. Since it is unlikely that two acid molecules would simultaneously encounter the common “atomic site” undergoing oxidation at the steel surface, it can be safely assumed that the reaction proceeds by consecutive interactions of acid molecules. Therefore, it can be inferred that the association of iron with an acid molecule forms the active intermediate  $\text{Fe}(\text{RCOOH})^*$  as a first step. Such chemical interaction of the carboxylic acid molecule with the surface site is shown below by elementary reaction B.<sup>31–34</sup>



In the second step, another acid molecule from the oil phase interacts with the active intermediate  $\text{Fe}(\text{RCOOH})^*$  forming iron carboxylate and hydrogen as per the below reaction C.<sup>26</sup>



These elementary steps are illustrated schematically in Figure 1.

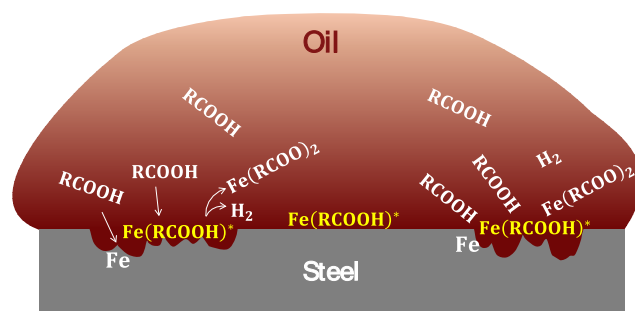


**Figure 1.** Mechanism of high-temperature oil-phase carboxylic acid corrosion of steel.

It is assumed that the elementary reaction C is unlikely to be reversible. An asterisk is used for the active intermediate to indicate insufficient stability of the bonding, which may not qualify as a metastable state. The method adopted for deciphering the corrosion reaction mechanism may seem analogous to the Lindemann–Hinshelwood mechanism due to formation of an active intermediate. However, the intermediate  $\text{Fe}(\text{RCOOH})^*$  is termed active due to insufficient stability of the bonds rather than being activated by a collision with some neutral molecule as per the Lindemann–Hinshelwood mechanism.<sup>35</sup> The qualitative Gibbs energy diagram for the proposed elementary reactions has been traced in Figure 2.<sup>36</sup>

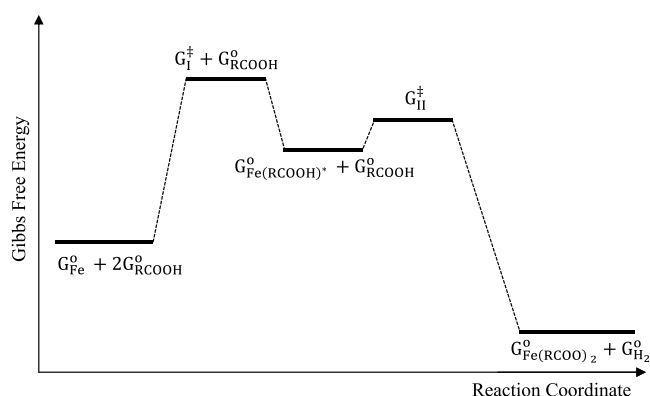


**Figure 2.** Gibbs free energy diagram of the corrosion reaction of iron with carboxylic acid.

The Gibbs energy diagram includes standard Gibbs energies of reactants, products and intermediates together with the Gibbs energies of the transition states for reactions B and C as indicated by  $G_I^{\ddagger}$  and  $G_{II}^{\ddagger}$ , respectively. Since the transition state of reaction B only involves one of the two acid molecules, the standard Gibbs energy of the unreacted molecule must be added to the activated state, i.e.,  $G_I^{\ddagger} + G_{\text{RCOOH}}^0$ , to count total Gibbs energy of the state.<sup>36</sup>

The mechanism given by reactions B and C is also applicable if carboxylic acid corrosion occurs in the vapor phase as long as there is some presence of iron carboxylate therein; there is limited literature available quantifying these phenomena.<sup>27,37</sup> The postulated mechanism is also applicable if the first and

second carboxylic acids are different, resulting simply in heteromorphous Fe(II) carboxylate.

Catalytic conversion of carboxylic acids to ketones by iron may also be observed in a certain lower temperature range instead of corrosion.<sup>23,24</sup> The selectivity of the reaction pathway between the formation of the active intermediate with iron or the catalytic conversion by iron should depend on the molecular structure of the acids and the temperature. Such catalytic conversion of carboxylic acids has been investigated by other workers and is not a part of the present work.<sup>23,24</sup>

Another potential pathway for the decay of active intermediate can be envisioned for higher temperatures that could result in the formation of iron oxide and aldehydes as shown below by reaction D.<sup>26</sup>



The presence of iron oxide in the form of magnetite Fe<sub>3</sub>O<sub>4</sub> has been observed experimentally, in parallel with carboxylic acid corrosion, which is suspected to be converted from FeO.<sup>38–40</sup> Current theory on the formation of iron oxides proposes their formation by thermal decomposition of iron carboxylates considering the presence of ketones in the solution as proof of the mechanism.<sup>38,39</sup> However, ketones cannot be considered the sole proof for the thermal decomposition mechanism since they can also be produced by catalytic conversion by metals and their oxides as mentioned before.<sup>23,24</sup> To the best of the authors' knowledge, before Jin *et al.*, the thermal decomposition mechanism had been proposed by other workers only as a hypothesis.<sup>26,39,41,42</sup> There is also a popular method for the production of nanosized Fe<sub>3</sub>O<sub>4</sub> particles through the thermal decomposition of Fe(III) carboxylates in a hydrocarbon environment.<sup>43–46</sup> However, Fe(II) carboxylates, which are generated during carboxylic acid corrosion, have never been used for such syntheses.<sup>26,43–46</sup> An alternative reaction pathway (D) is thus proposed here for the formation of iron oxide as a byproduct generated from the decay of the active intermediate.<sup>26</sup> The main idea here is that the source of oxygen is the acid molecule rather than the iron carboxylate. However, it is still debatable if the actual reaction pathway for the formation of iron oxide could involve fast transition via an activated complex instead of an active intermediate that persists for longer durations.

**Kinetics.** The reaction rate law for high temperature carboxylic acid corrosion can be derived as follows. The mechanism proposed in the previous section consists of two elementary steps for which the simple rate equations could be written according to chemical kinetics. The rate law for the formation of the intermediate in reaction 1 can be written as follows.

$$r_1 = k_1C - k_{-1}C^* \quad (1)$$

Here,  $r_1$  is the rate of formation of Fe(RCOOH)\* in mol·m<sup>-2</sup>·s<sup>-1</sup>,  $k_1$  is the rate constant for the forward reaction in m·s<sup>-1</sup>,  $C$  is the concentration of RCOOH in bulk fluid in mol·m<sup>-3</sup>,  $k_{-1}$  is the rate constant for the backward reaction in eq 1 in s<sup>-1</sup>, and  $C^*$  is the surface concentration of active intermediate Fe(RCOOH)\* in mol·m<sup>-2</sup>.

The elementary rate law for consumption of the intermediate in reaction C can be written as shown below.

$$r_2 = k_2CC^* \quad (2)$$

Here,  $r_2$  is the rate of consumption of Fe(RCOOH)\* in the second step (C) or the rate of formation of Fe(RCOO)<sub>2</sub> in mol·m<sup>-2</sup>·s<sup>-1</sup>, and  $k_2$  is the rate constant in m<sup>3</sup>·s<sup>-1</sup>·mol<sup>-1</sup>.

At this point in the derivation, the net rates of formation or consumption of each of the reactants and products involved in the elementary reactions in the differential form are expected to be written to determine the evolution of concentrations and thus reaction rates. However, the purpose here is to derive a simple and useful rate law for the overall reaction of carboxylic acid corrosion, which can be validated experimentally. Therefore, it is assumed that the active intermediate Fe(RCOOH)\* is in a pseudo-steady state such that its concentration does not change significantly with time, which means that the net rate of formation of Fe(RCOOH)\* is close to zero or at least insignificant compared to the rate of formation of iron carboxylates.<sup>47</sup> The pseudo-steady state hypothesis (PSSH) is a useful approximation, which makes it easier to solve the eqs 1 and 2 without using a system of differential equations.<sup>47</sup>

$$r^* = r_1 - r_2 \approx 0$$

here,  $r^*$  = net rate of formation of Fe(RCOOH)\* in mol·m<sup>-2</sup>·s<sup>-1</sup>

Substituting the values of  $r_1$  and  $r_2$  from equations (1) and (2) into the above equation,

$$k_1C - k_{-1}C^* - k_2CC^* = 0$$

$$k_1C - k_{-1}C^* - k_2CC^* = 0$$

$$\therefore C^* = k_1C / (k_{-1} + k_2C) \quad (3)$$

It can be observed from eq 3 that the concentration of the active intermediate is an asymptotic function with a horizontal asymptote of  $k_1/k_2$ , which is the maximum concentration of the active intermediate. Qualitatively speaking, a higher acid concentration pushes the active intermediate to the concentration of  $k_1/k_2$  mol·m<sup>-2</sup>·s<sup>-1</sup>, which indicates the "highest" surface coverage. The highest surface coverage does not mean that surface would "saturate" because increasing bulk acid concentration still increases the corrosion rate despite achieving high coverage, as experimentally demonstrated further.

The rate of formation of iron carboxylates  $r_2$  can be considered as an indicator of the corrosion rate, as warranted by this mechanism. Therefore, from eqs 2 and 3, a corrosion rate of steel by carboxylic acids can be determined as shown below.

$$r_2 = k_1k_2C^2 / (k_{-1} + k_2C) \quad (4)$$

Equation 4 has an oblique asymptote, which approximates the corrosion rate to the linear function of  $r_2 = k_1C - (k_1k_{-1}/k_2)$  as the acid concentration goes higher, which is also experimentally observed herein. The validation of the rate in eq 4 is demonstrated further in the experimental section.

Carboxylic acid corrosion is accompanied by sulfide corrosion in refinery distillation units. Since the sulfidation corrosion produces solid iron sulfide scale, carboxylic acids shall diffuse through the porosity of the scale as illustrated in Figure 3. Nonetheless, the mechanism of the corrosion reaction should remain the same. The molecular diffusion of acids through iron sulfide scale has already been modeled elsewhere.<sup>48,49</sup>

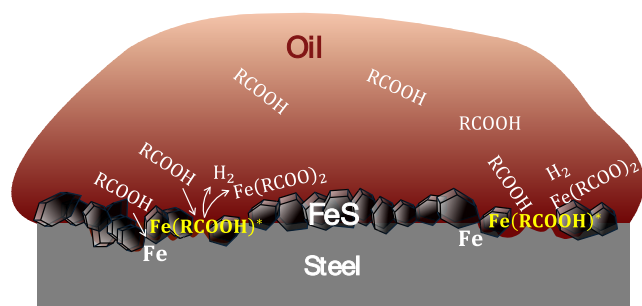


**Figure 3.** Carboxylic acid corrosion of steel in the presence of iron sulfide, formed by concurrent sulfidation corrosion.

## MATERIALS AND METHODS

**Experimental Methodology.** Although the concurrent phenomenon of sulfidation corrosion may influence the carboxylic acid corrosion reaction A,<sup>50–52</sup> the postulate behind choosing an isolated experimental study of carboxylic acid corrosion is that the reaction mechanism should be preserved, at least partially, when combined with sulfidation corrosion.

All corrosion experiments were conducted in flow-through reactors in this work to avoid computational corrections for depletion and accumulation of acids and carboxylates, respectively. These reactors were a flow through mini autoclave (FTMA)<sup>50</sup> and a high velocity rig (HVR).<sup>49,51,53</sup> Kinetic control is promoted by fluid velocity in the flow through reactors by enhancing the convection of acids and iron carboxylates. The solvation of iron carboxylates was assumed to be rapid considering their high solubility, and convective mass transport facilitated in the flow-through reactors.

A mixture of petroleum-derived carboxylic acids was used as a model carboxylic acid for the corrosion experiments which could act as a good representative of the acid composition of crude oil.<sup>38</sup> This mixture also produced consistent corrosion rates, with the increase in temperature indirectly indicating lower decomposition rates. Specific model carboxylic acid molecules have been used and reveal the same kinetics, as demonstrated by the literature data.<sup>1,19,26,27,29,30</sup>

Some secondary processes occur in parallel with high-temperature carboxylic acid corrosion. Carboxylic acids partition into the vapor phase.<sup>27,54</sup> In addition, they undergo thermal<sup>18,19,21,22</sup> and catalytic decomposition.<sup>23,24,41,55</sup> The oil-soluble iron carboxylates derived from corrosion are also presumed to decompose thermally.<sup>42,56</sup> Due to this, neither the acid consumption rate nor the carboxylate formation rate can be used as a proxy for the corrosion reaction rate as their thermal decomposition restricts the validity of *in situ* measurement of concentrations. Hence, the rate of mass loss of steel is used here as an indicator of the experimental corrosion rate. Corrosion rates calculated using mass loss measurements during

corrosion experiments are plotted versus concentration and temperature.

The primary objective of the experimental study was to investigate the underlying reaction mechanism of carbon steel corrosion caused by carboxylic acids in the crude oil. Therefore, the corrosion experiments were performed in the flow-through reactors, which kept the convective mass transfer coefficient of corrosive molecules high enough so that mass transfer was not the rate limiting step. Carboxylic acid corrosion does not produce significant scale, hence, its rate remains constant over time; this is supported by experimental data in the literature.<sup>57</sup> The negligible fraction of sulfur in the model acid mixture produced a thin iron sulfide layer on the surface of the specimens, but virtually no corrosion protection was offered by the layer and the metal dissolution could be considered being governed by redox process A. The flow reactor avoided the accumulation or depletion of reactants and products in the experimental environment. Also, the relatively lower residence time, approximately 3 min at peak temperature, of the oil solution in the flow reactor at high temperatures restricted the thermal decomposition of acids. However, it was infeasible to measure decomposition rates due to instrumental limitations.

The manipulated variables in the kinetic investigation included time, concentration, and temperature. The measurement of corrosion rate versus a series of concentrations was done to determine the order of reaction as well as the mechanism. The measurement of the corrosion rate versus a series of temperatures was done to determine the reaction kinetics.

**Equipment. Flow-Through Mini Autoclave (FTMA).** Two sets of corrosion experiments, corrosion rate versus concentration and temperature, were performed in the flow-through mini autoclave (FTMA) as illustrated schematically in Figure 4.<sup>53,59</sup> The FTMA setup consists of a high temperature and high pressure reactor, two feeding tanks, separate pumps for feeding oil solution, and a waste tank. The test solution containing the model acids was supplied from the feed tank for corrosion of steel specimens and paraffinic mineral oil from the flush tank for preheating and flushing. A three-way valve was utilized for switching the oil feeds. The temperature was measured by a thermocouple inserted into the reactor near the specimens. The thermocouple and heating coil around the reactor were connected to the temperature controller. The pressure inside the reactor was controlled by a back-pressure valve at the outlet of the reactor to maintain a full liquid phase.<sup>59</sup>

**High Velocity Rig (HVR).**<sup>49</sup> Another set of experiments on corrosion rate versus concentration series was conducted in a high velocity rig (HVR) as illustrated in Figure 5. This system included an enclosed autoclave, a metering pump, a feeding tank filled with the test solution, a flushing tank with mineral oil, an electromagnetic valve, a preheater located between the pump and autoclave, and a waste drum at the outlet of the autoclave. The experiment temperature was maintained using electric heating elements, including

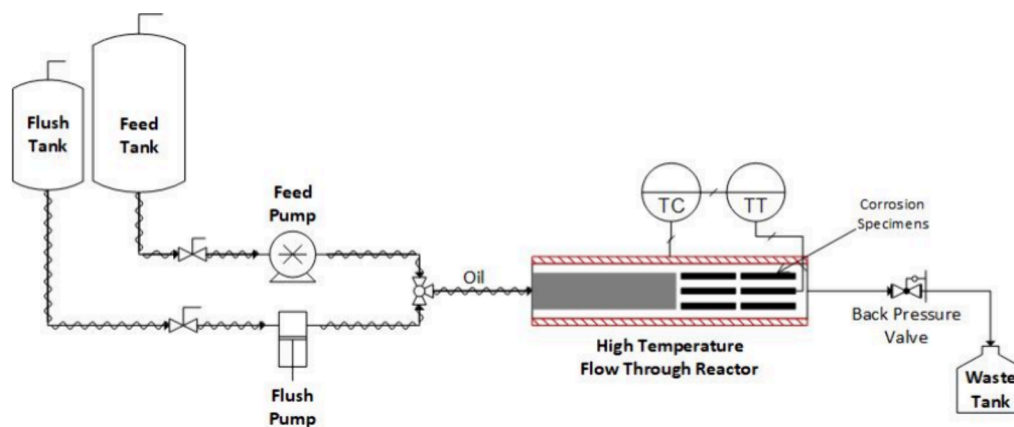


**Figure 4.** Schematic diagram of the flow through mini autoclave (FTMA).<sup>53,58,59</sup>

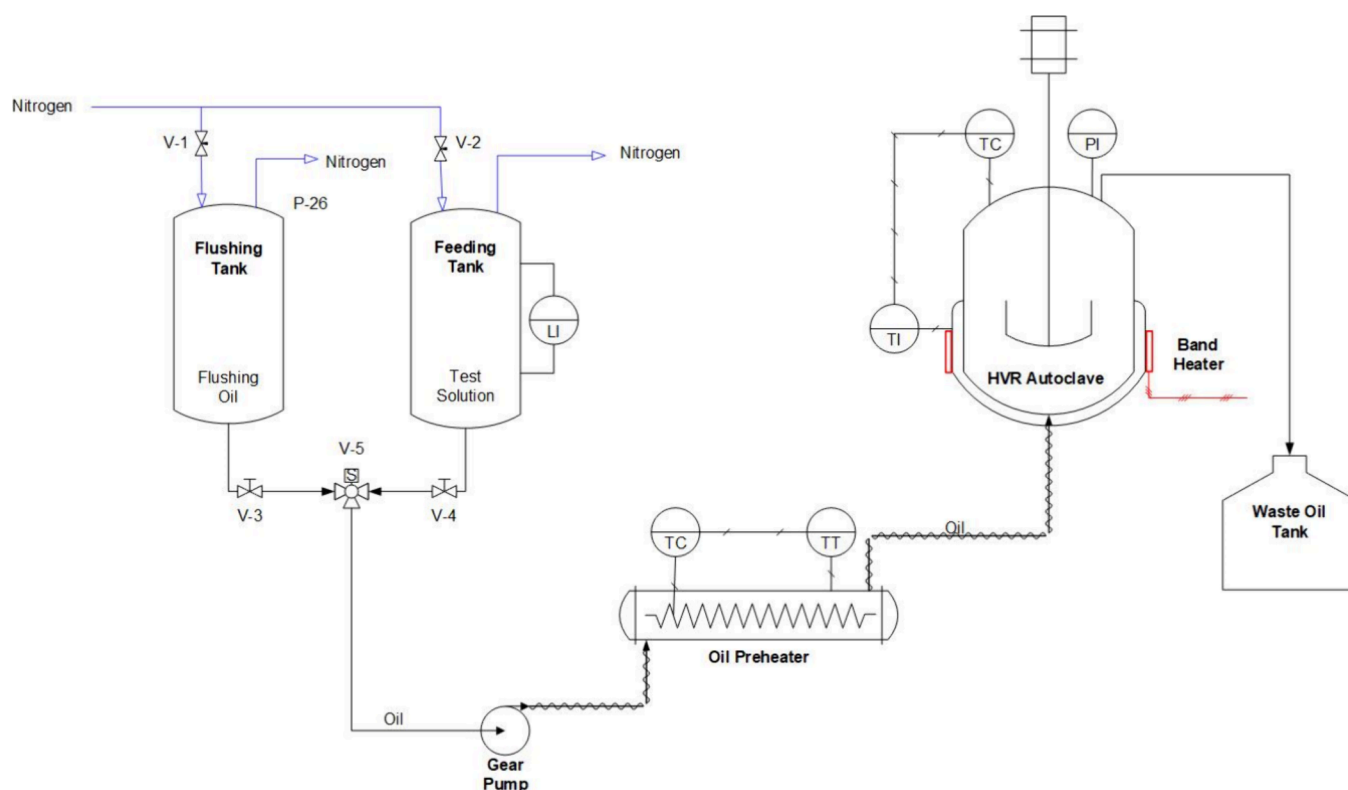


Figure 5. Schematic diagram of the high velocity rig (HVR).<sup>50</sup>

Table 1. Chemical Composition (wt.%) of Carbon Steel Specimens<sup>53</sup>

C	Si	Mn	P	S	Cr	Ni	Mo	V	Cu	Fe
0.18	0.41	0.8	0.11	0.06	0.02	0.04	0.02	0.03	0.08	balance

two-ring electric heaters for the autoclave vessel and electric tape for other rig components. The autoclave had a rotor for attaching the ring specimens, which were rotated at high angular velocity to increase convective mass transport of corrosive molecules. Test solution was introduced into the autoclave through a bottom inlet, and the pump's flow rate was adjusted via the control panel.

**Analytical Instruments.** A JEOL JSM-6390 scanning electron microscope (SEM) was used to analyze the surface scale structure and morphology. EDS elemental analysis of the scale cross-section was performed using a Bruker energy-dispersive spectroscopy (EDS) analyzer. X-ray diffraction patterns for the solid corrosion products were collected with a Rigaku Miniflex 600 X-ray diffractometer.

**Materials.** All model oil solutions were prepared in the paraffinic mineral oil Tufflo 6056 (Citgo). The model acids used to induce carboxylic acid corrosion were a mixture of naturally occurring acids extracted from a crude oil distillation side cut supplied by TCI America (purity of >97%), this contains a trace of sulfur (0.071 wt %, measured by X-ray fluorescence spectroscopy using a XOS Petramax instrument).<sup>17</sup> Concentrations of the model oil solutions are specified using total acid number (TAN), which is the milligrams of KOH required to neutralize the acids in a gram of oil. Four rectangular carbon steel corrosion specimens of specific length, width, thickness, and central hole diameter were used in each experiment with the FTMA. The HVR experiments used ring specimens of carbon steel with outside and inside diameters of 81.76 and 70.43 mm, respectively, and a height of 5 mm. The chemical compositions of carbon steel specimens is given in Table 1. Both rectangular and ring specimens were sequentially polished with Indasa Rhynogrip White Line 400 and 600 grit abrasive papers under a continuous flow of isopropyl alcohol and dried by blowing pure CO<sub>2</sub> or N<sub>2</sub>. The dimensions of each specimen were measured by a caliper, and their weights taken using a XPR205 Mettler Toledo analytical balance. At

the end of each experiment, one of the specimens was mounted in epoxy and polished for cross-section SEM-EDS analyses.

**Experimental Matrices.** The proposed corrosion reaction rate law, eq 4, was validated by performing experiments of corrosion rate versus concentration by keeping the other parameters constant, as listed in Tables 2 and 3. The effect of the temperature on the corrosion rates was evaluated by a set of experiments listed in Table 4.

Table 2. Evaluation of the Corrosion Rate of Carbon Steel in FTMA with Respect to Acid Concentration

concentration of the model acids solution in mineral oil TAN (mg of KOH/g of oil)	corrosion specimens	temperature (°C)	pressure (kPa)	time (h)
0.25	carbon steel <sup>53</sup>	343	600	24
0.50				
1.00				
1.50				
2.00				
4.00				

**Experimental Procedure. FTMA Experiments.** The test solution for each experiment was prepared in a 2 L glass beaker by adding the mixture of specific concentrations of model acids in the mineral oil. The solution was stirred using a glass rod until it was uniform in color. The solution was poured into the feed tank of FTMA well in advance of each experiment to let the air bubbles slowly escape the solution.

Each experiment utilized four carbon steel specimens of known weight and dimensions: two for the mass loss, one for surface analysis by SEM and XRD, and one for cross-section analysis by SEM and EDS. Specimens were prepared by polishing with 400 and 600 grit

**Table 3. Evaluation of Corrosion Rate of Carbon Steel in HVR with Respect to Acid Concentration**

concentration of the model acids solution in mineral oil TAN (mg of KOH/g of oil)	corrosion specimens	temperature (°C)	pressure (kPa)	time (h)	specimen rotation speed (RPM)
0.10	carbon steel <sup>53</sup>	343	3450	24	2000
2.00					
3.50					
5.00					
6.50					
8.00					

**Table 4. Evaluation of the Carboxylic Acid Corrosion Rate in FTMA with Respect to Temperature**

temperature (°C)	concentration of the model acids solution in mineral oil TAN (mg of KOH/g of oil)	corrosion specimens	pressure (kPa)	time (h)
288	3.5	carbon steel <sup>53</sup>	600	24
316				
343				

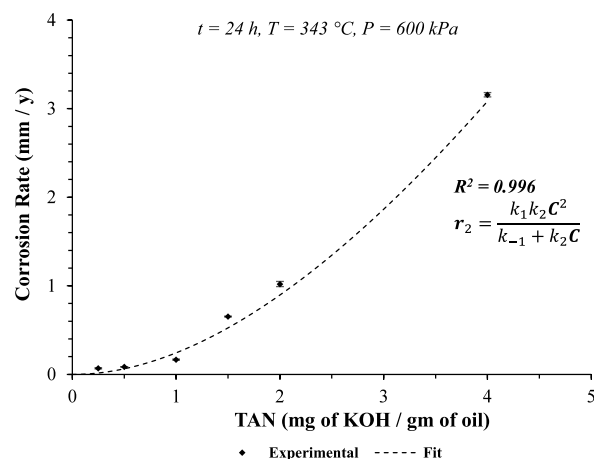
polishing papers, respectively, using isopropanol. Specimens were placed on the holder and loaded into the FTMA reactor. The reactor was connected to the FTMA loop. In the first phase of operation, the reactor was run cold by pumping mineral oil using a positive displacement pump to fill the reactor and all the lines. In the second phase, the electric heating coil was powered and the reactor temperature was raised in small steps to 343 °C while still flowing mineral oil. Once the required temperature was reached, the third phase was started by switching the feed from the mineral oil to the test solution. In the fourth phase at the end of the test duration, the feed was switched back to mineral oil for flushing for 1 h and then the reactor was turned off while letting mineral still run through the reactor to aid cooling. Finally, the system was turned off after 10 min.

After the reactor cooled to room temperature, corrosion specimens were extracted and cleaned carefully by stepwise dipping in toluene while still retaining solid corrosion product on the surface. The mass of each of the two specimens was measured dry, then after rubbing off loosely adherent solid corrosion product, and after chemically removing strongly adherent corrosion products by Clarke solution according to ASTM G1–03. The corrosion rate was determined by dividing the average difference in the initial and final masses of the two specimens by the experiment duration. The third specimen was taken for the surface analysis, and the fourth one was embedded in the epoxy for the analysis of the cross-section.

**HVR Experiments.**<sup>49</sup> The ring-type corrosion specimens were inserted in the autoclave to start the phasewise operation of HVR. In the first phase, the lines and the autoclave were filled with mineral oil at the pressure of 3450 kPa and then the rotor was started. In the second phase, the temperature was raised in steps from room temperature to 343 °C through a temperature control panel. The system was held isothermally for 30 min after reaching the experiment temperature. In the third phase, the feed was changed from the mineral oil to the test solution using an electromagnetic valve of the rig to let the ring specimens corrode with the test solution. At the end of the test duration, the feed was switched back from the test solution to mineral oil for flushing. In the final flushing phase, heated white oil was pumped into the rig for cleaning purposes. In the end, heating elements were turned off while still letting the mineral oil run through for 30 min to let the system cool to room temperature. The corrosion specimens were processed for mass loss in the same manner as that for the FTMA specimens.

## RESULTS AND DISCUSSION

Average corrosion rates of carbon steel specimens in FTMA experiments are plotted against the concentration of the model acid solution. The trend of corrosion rate accurately validates the derived rate law in eq 4, as shown in Figure 6. The rate

**Figure 6.** Validation of the derived rate law, eq 4, by experimental carbon steel corrosion rates versus concentrations of acids in FTMA.

constants are not reported because the reported value would just be representative for a mixture of carboxylic acids. Almost second-order kinetics can be observed at lower concentrations, which gradually approaches first order kinetics at higher concentrations. Such a “transition” from second- to first-order kinetics was also noted by Hauet *al.*, for carboxylic acid corrosion of iron, although the experimental methodology was quite different than adopted herein.<sup>60</sup> It should be noted that such a gradual transition does not represent the shift of control from mass transfer to reaction kinetics with an increasing concentration. The mass transport-controlled reaction rate linearly depends on concentration, especially for lower concentrations. Moreover, mass transport control depends on the velocity of the solution rather than concentration. Hence, it can be inferred that the nonlinear trend of corrosion rate versus concentration observed in FTMA experiments indicates reaction control.

In the HVR experiments, the high-speed rotation of ring specimens relative to the stationary solution enhances convective mass transport of acid molecules. The corrosion rates of ring specimens plotted against concentration of acids in Figure 7 shows the first-order reaction kinetics. Similar first-order kinetics for high temperature carboxylic acid corrosion has been observed by several other researchers.<sup>1,19,26,27,29,30</sup> This can be derived from eq 4 as  $r_2 \approx k_1 C$  for condition  $k_2 C \gg k_{-1}$ . It is suspected that this condition becomes effective for HVR experiments due to higher operating pressure. A more accurate asymptotic approximation would still be  $r_2 = k_1 C - k_1 k_{-1} / k_2$  as derived earlier. The intercept  $k_1 k_{-1} / k_2$  on the abscissa is negligible for the HVR experimental data in Figure 7.

The temperature dependency of the reaction rate can be evaluated by plotting the unit rate on an Arrhenius plot, as illustrated in Figure 8. The concentration of TAN 3.5 used for this series of experiments was considered in the range of first-order kinetics. The activation energy of 46.5 kJ/mol

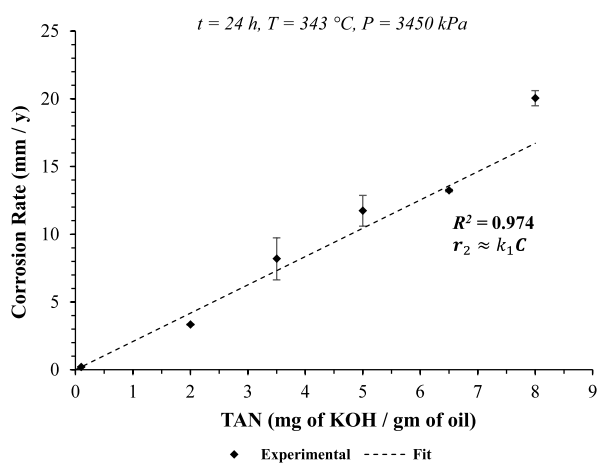


**Figure 7.** Experimental corrosion rate data of carbon steel specimens versus the concentration of acid in HVR showing “first-order” kinetics ( $r_2 \approx k_1 C$ ), a corollary of the derived rate law.

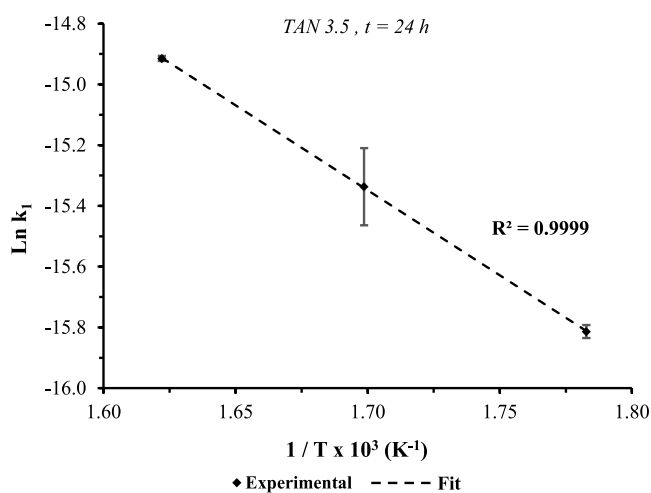


**Figure 8.** Arrhenius plot of the first-order kinetics. Carbon steel specimens were exposed to the solution of commercial model acid mixture in mineral oil in the FTMA.<sup>53</sup>

determined from the slope of the plot is an average representative value for the mixture of model acids.

As mentioned earlier, the test solution contains traces of sulfur, which could potentially generate an iron sulfide film on the surface of corrosion specimens. Also, there is the formation of iron oxides of different crystal structures during high temperature carboxylic acid corrosion. Therefore, these solid products on the surface of corrosion specimens were analyzed at the end of each FTMA experiment by using scanning electron microscopy (SEM) for morphology, energy-dispersive spectroscopy (EDS) for chemical composition, and X-ray diffraction (XRD) for crystallinity and solid-phase identification. The geometry of specimens from HVR experiments was not as suitable for these analyses. It is important to note that the purpose of such analyses is not quantification of the phase composition but rather to judge the effect of solid products on the corrosion rates.

SEM analyses of FTMA corrosion specimens with solid products revealed that their surfaces were covered by solids of different morphologies and sizes, as shown in Figure 9. The outward growth of the products was exhibited in several cases

by the newly formed clusters of crystals. Minor phases were occasionally observed, too.

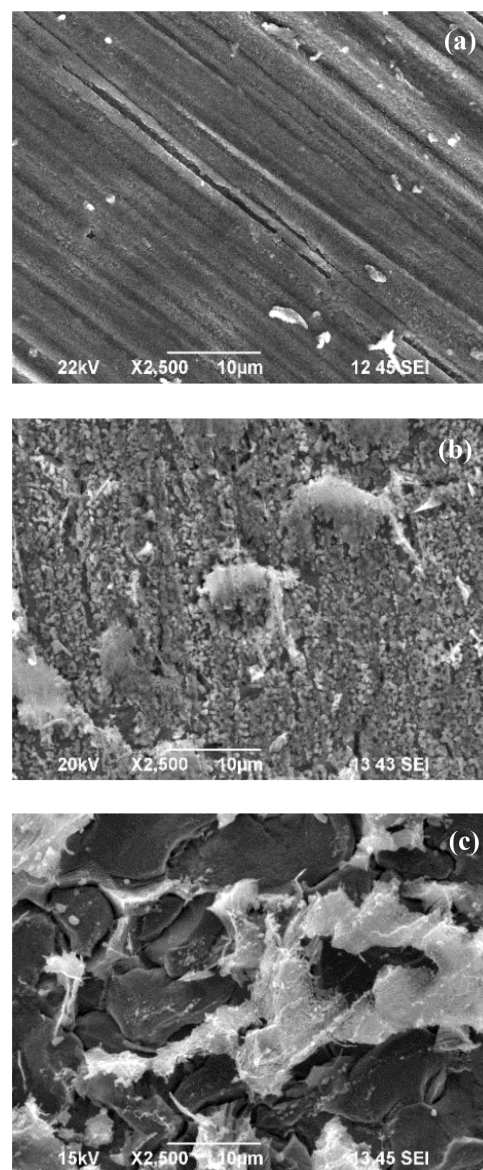


**Figure 9.** SEM morphological analyses of solid corrosion products on carbon steel specimens corroded for 24 h at 343 °C by acid concentrations: (a) TAN 0.5; (b) TAN 2; and (c) TAN 4.

EDS data from solid products on FTMA corrosion specimens are shown in Figure 10, iron sulfide and iron oxide were detected. The atomic percentages are not so reliable because, for an applied acceleration voltage, EDS analysis depends on the depth of the interaction volume from where the characteristic X-rays are produced; which limits the interpretation of data. To address this shortcoming, EDS analyses were performed on the cross sections of specimens, as shown in Figure 11. The main elements Fe, O, S and C were detected in both surface as well as cross-sectional analyses which implied the presence of iron oxide and iron sulfide phases.

The effect of a thin iron sulfide layer on carboxylic acid corrosion was evaluated in an exaggerated corrosion experiment of high TAN 5.5 in FTMA for 7 days. It showed that the

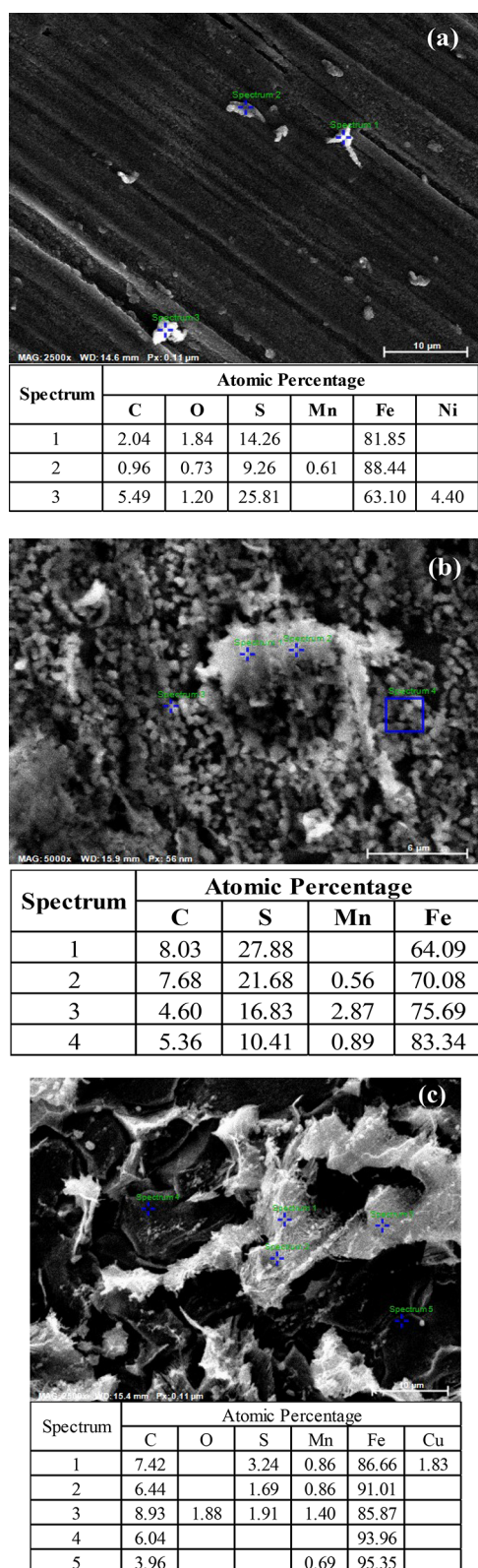


**Figure 10.** EDS chemical analyses of solid corrosion products on carbon steel specimens corroded for 24 h at 343 °C by acid concentrations: (a) TAN 0.5; (b) TAN 2; and (c) TAN 4.

trace amount of sulfur in TCI acids is unable to provide any barrier to carboxylic acid corrosion, and it did not grow. The SEM micrograph of cross-section of the corroded sample is shown in Figure 12. It is evident that carboxylic acids

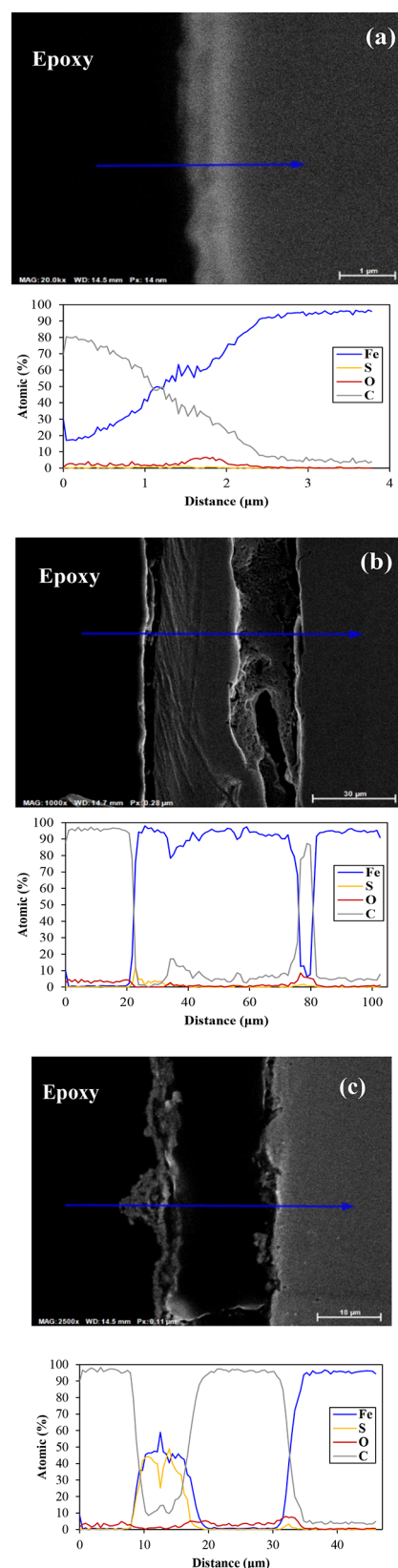


**Figure 11.** EDS chemical analyses of cross section of FTMA corrosion specimens corroded for 24 h at 343 °C by acid concentrations: (a) TAN 0.5; (b) TAN 2; and (c) TAN 4.

penetrated through the thin iron sulfide layer to dissolve the metal. A skeleton-like morphology left behind during

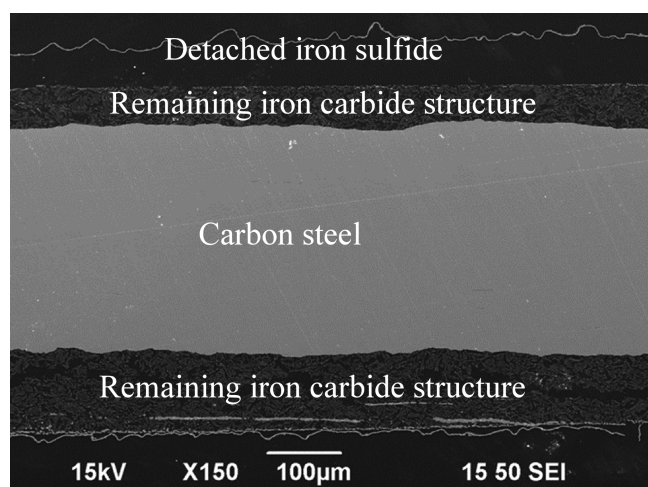


**Figure 12.** SEM cross section of the carbon steel specimen corroded by TCI acid solution of TAN 5.5 for 7 days.

dissolution of the metallic phase is iron carbide, a strengthening phase in carbon steel. The iron sulfide layer got detached due to the stresses generated during epoxy curing.

Crystallinity of the phases in the solid corrosion products was analyzed by X-ray diffraction (XRD). The diffraction data for each specimen were collected at a scanning speed of 3 degrees per minute, with a step width of  $0.02^\circ$  using  $\text{CuK}\alpha$  radiation produced at 30 kV and 15 mA. The identified peaks in the pattern corresponded to  $\alpha$ -Fe (ferrite), FeS (troilite) (PDF 01-075-8714),<sup>61</sup>  $\text{Fe}_2\text{O}_3$  (maghemite) (PDF 00-039-1346),<sup>61</sup> and  $\text{Fe}_3\text{C}$  (cohenite) as shown in Figure 13. No

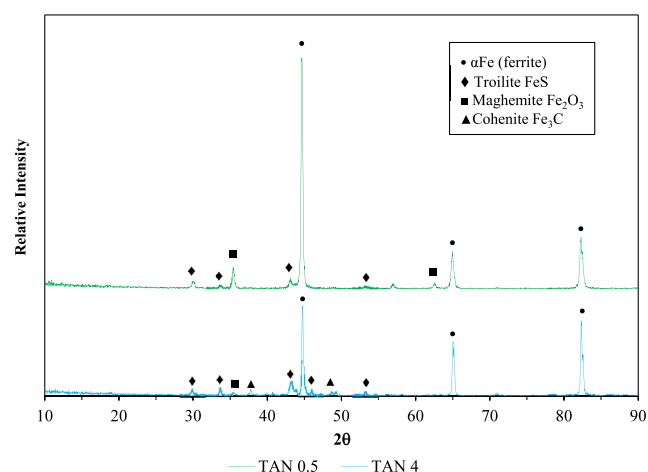


**Figure 13.** Phase identification of solid products on the surface of corrosion specimens corroded for 24 h at 343 °C by the model solutions of concentrations TAN 0.5 and TAN 4.

amorphous phases were observed in any of the specimens. It should be noted that the stoichiometry of iron sulfide and iron oxide may vary depending on the concentration of the solution, which would show up as a shift in the peak position. For example, the XRD peaks for iron oxide fitted more accurately with maghemite which is an end member of nonstoichiometric magnetite. This also supports the presented hypothesis that the formation of iron oxide is a result of an oxidation process rather than thermal decomposition.

## CONCLUSIONS

The mechanism of high temperature carboxylic acid corrosion was proposed by positing the formation of an active intermediate that aided in splitting the heterogeneous reaction into elementary steps. The reaction rate law for the overall corrosion reaction was derived using an approximation of the pseudo-steady state hypothesis. Experimental corrosion data validated this rate law. The “first-order” kinetics reported herein and by several other researchers emerged as a corollary of the derived rate law.

## AUTHOR INFORMATION

### Corresponding Author

David Young – Institute for Corrosion and Multiphase Technology, Ohio University, Athens, Ohio 45701, United States; [orcid.org/0000-0002-1077-9586](https://orcid.org/0000-0002-1077-9586); Phone: +1-740-593-9944; Email: [youngd1@ohio.edu](mailto:youngd1@ohio.edu)

### Authors

Ishan P. Patel – Institute for Corrosion and Multiphase Technology, Ohio University, Athens, Ohio 45701, United States

Gheorghe Bota – Institute for Corrosion and Multiphase Technology, Ohio University, Athens, Ohio 45701, United States

Peng Jin – Institute for Corrosion and Multiphase Technology, Ohio University, Athens, Ohio 45701, United States; [orcid.org/0000-0002-9318-0498](https://orcid.org/0000-0002-9318-0498)

Complete contact information is available at:

<https://pubs.acs.org/10.1021/acs.energyfuels.4c01284>

### Author Contributions

<sup>†</sup>Baker Hughes, 12645 W Airport Blvd, Sugar Land, Texas 77478, United States

### Author Contributions

The manuscript was written through contributions of all authors. All authors have given approval to the final version of the manuscript.

### Notes

The authors declare no competing financial interest.

## ACKNOWLEDGMENTS

This work was supported by Naphthenic Acid Corrosion Joint Industry Project (NAP JIP) in the Institute for Corrosion and Multiphase Technology, Ohio University.

## REFERENCES

- Slavcheva, E.; Shone, B.; Turnbull, A. Review of Naphthenic Acid Corrosion in Oil Refining. *Br. Corros. J.* **1999**, *34* (2), 125–131.
- U.S. Energy Information Administration (EIA). *Short-Term Energy Outlook*; 2024. <https://www.eia.gov/outlooks/steo/>.
- Chakravarthy, R.; Naik, G. N.; Savalia, A.; Sridharan, U.; Saravanan, C.; Das, A. K.; Gudasi, K. B. Determination of Naphthenic Acid Number in Petroleum Crude Oils and Their Fractions by Mid-Fourier Transform Infrared Spectroscopy. *Energy Fuels* **2016**, *30* (10), 8579–8586.
- Eschenbacher, A.; Myrstad, T.; Bech, N.; Thi, H. D.; Auersvald, M.; Van Geem, K. M.; Jensen, A. D. Fluid Catalytic Co-Processing of Bio-Oils with Petroleum Intermediates: Comparison of Vapour Phase Low Pressure Hydrotreating and Catalytic Cracking as Pretreatment. *Fuel* **2021**, *302*, No. 121198.
- Pinho, A. de R.; de Almeida, M. B. B.; Mendes, F. L.; Casavechia, L. C.; Talmadge, M. S.; Kinchin, C. M.; Chum, H. L. Fast Pyrolysis

- Oil from Pinewood Chips Co-Processing with Vacuum Gas Oil in an FCC Unit for Second Generation Fuel Production. *Fuel* **2017**, *188*, 462–473.
- (6) Marker, T.; Petri, J.; Kalnes, T.; McCall, M.; Mackowiak, D.; Jerosky, B.; Reagan, B.; Nemeth, L.; Krawczyk, M.; Czernik, S.; Elliott, D.; Shonnard, D. *Opportunities for Biorenewables in Oil Refineries*; DOE F 241.3; 25 East Algonquin Road Des Plaines, Illinois 60017–5017, 2005 <https://www.osti.gov/biblio/861458>. DOI: [10.2172/861458](https://doi.org/10.2172/861458).
- (7) Lindfors, C.; Elliott, D. C.; Prins, W.; Oasmaa, A.; Lehtonen, J. Co-Processing of Biocrudes in Oil Refineries. *Energy Fuels* **2023**, *37* (2), 799–804.
- (8) Official Journal of the European Union *Directive (EU) 2018/2001 of The European Parliament and of the Council of 11 December 2018 on the promotion of the use of energy from renewable sources*, Issued on 2018–12–21. <https://eur-lex.europa.eu/eli/dir/2018/2001/oj>.
- (9) Environmental Protection Agency, RIN 2060–AV14, *Renewable Fuel Standard (RFS) Program: Standards for 2023–2025 and Other Changes*, Issued on 2023–07–12, Effective 2023–09–11, Federal Register/Vol. 88, No. 132. <https://www.federalregister.gov/documents/2023/07/12/2023-13462/renewable-fuel-standard-rfs-program-standards-for-2023-2025-and-other-changes>.
- (10) Brady, M. P.; Keiser, J. R.; Leonard, D. N.; Zacher, A. H.; Bryden, K. J.; Weatherbee, G. D. Corrosion of Stainless Steels in the Riser during Co-Processing of Bio-Oils in a Fluid Catalytic Cracking Pilot Plant. *Fuel Process. Technol.* **2017**, *159*, 187–199.
- (11) Brady, M. P.; Leonard, D. N.; Keiser, J. R.; Cakmak, E.; Whitmer, L. E. Degradation of Components After Exposure in a Biomass Pyrolysis System. In *CORROSION 2019, Proceedings of Corrosion Issues in the Pulp, Paper, and Biomass Conversion Industries Symposium*, NACE International, Publications Division: Nashville, Tennessee, USA, 2019, C2019–13446.
- (12) Babaian-Kibala, E.; Craig, H. L., Jr.; Rusk, G. L.; Blanchard, K. V.; Rose, T. J.; Uehlein, B. L.; Quinter, R. C.; Summers, M. A. Naphthenic Acid Corrosion in Refinery Settings. *Mater. Perform.* **1993**, *50*–55.
- (13) Groysman, A.; Naphtali, B.; Penev, J.; Goldis, A.; Savchenko, N. Study of Corrosiveness of Acidic Crude Oil and Its Fractions. In *CORROSION 2005*, NACE International, Publications Division: Houston, TX, USA, 2005, NACE-05568.
- (14) Clemente, J. S.; Prasad, N. G. N.; MacKinnon, M. D.; Fedorak, P. M. A Statistical Comparison of Naphthenic Acids Characterized by Gas Chromatography–Mass Spectrometry. *Chemosphere* **2003**, *50* (10), 1265–1274.
- (15) Clemente, J. S.; Fedorak, P. M. A Review of the Occurrence, Analyses, Toxicity, and Biodegradation of Naphthenic Acids. *Chemosphere* **2005**, *60* (5), 585–600.
- (16) Cason, J.; Graham, D. W. Isolation of Isoprenoid Acids from a California Petroleum. *Tetrahedron* **1965**, *21* (2), 471–483.
- (17) Hsu, C. S.; Dechert, G. J.; Robbins, W. K.; Fukuda, E. K. Naphthenic Acids in Crude Oils Characterized by Mass Spectrometry. *Energy Fuels* **2000**, *14* (1), 217–223.
- (18) Kapusta, S. D.; Ooms, A.; Smith, A.; Fort, W. C. Safe Processing of High Acid Crudes. In *CORROSION 2004*, NACE International, Publications Division: New Orleans, Louisiana, 2004; NACE-04637.
- (19) Turnbull, A.; Slavcheva, E.; Shone, B. Factors Controlling Naphthenic Acid Corrosion. *Corrosion* **1998**, *54* (11), 922–930.
- (20) Kane, R.; Cayard, M. S. Understanding Critical Factors, That Influence Refinery Crude Corrosiveness. *Mater. Perform.* **1999**, *48*–54.
- (21) Blum, S. C.; Olmstead, W. N.; Bearden, R., Jr.; Thermal Decomposition of Naphthenic Acids. EP0809683B1, 2001.
- (22) Busto, M.; Vera, C. R. Non-Catalytic Thermal Decomposition of Naphthenic Acids of Petroleum Crudes. *Braz. J. Chem. Eng.* **2022**, *39* (1), 105–112.
- (23) Gooßen, L. J.; Gooßen, K.; Rodríguez, N.; Blanchot, M.; Linder, C.; Zimmermann, B. New Catalytic Transformations of Carboxylic Acids. *Pure Appl. Chem.* **2008**, *80* (8), 1725–1733.
- (24) Gooßen, L. J.; Mamone, P.; Oppel, C. Catalytic Decarboxylative Cross-Ketonisation of Aryl- and Alkylcarboxylic Acids Using Magnetite Nanoparticles. *Adv. Synth. Catal.* **2011**, *353* (1), 57–63.
- (25) Li, X.; Binnemans, K. Oxidative Dissolution of Metals in Organic Solvents. *Chem. Rev.* **2021**, *121* (8), 4506–4530.
- (26) Patel, I.; Bota, G.; Young, D. Physicochemical Description of Refinery High Temperature Naphthenic Acid Corrosion. In *AMPP Annual Conference + Expo 2024, Proceedings of Oil Refining Industry Corrosion Symposium*, New Orleans, Louisiana, 2024; C2024–20988.
- (27) Gutzeit, J. Naphthenic Acid Corrosion in Oil Refineries. *Mater. Perform.* **1977**, *24*–35.
- (28) Wing, A.; Robbins, W.; Buchheim, G.; Sapienza, F. Introducing an Innovative Simultaneous Naphthenic Acid, Sulfidation and Mass Transport Corrosion Model for Crudes and Sidestreams. In *CORROSION Virtual Conference & Expo 2021*, 2021; NACE-2021-16755, D081S032R006.
- (29) Andari, F.; Kittel, J.; Fernandes, J.; Godin, N.; Ter-Ovanesian, B.; Ropital, F. High Temperature Corrosion in Various Grades of Vegetable and Waste Oils Used for Bio-Fuel Production. *Corros. Sci.* **2022**, *206*, No. 110501.
- (30) Hau, J. L.; Yepez, O.; Torres, L.; Specht, M. I. Classifying Crude Oils According to Corrosivity Using the Fe-Powder Test. In *CORROSION 2000*, NACE International, Publications Division: Orlando, Florida, USA, 2000; NACE-00699.
- (31) Pedersen, S.; Herek, J. L.; Zewail, A. H. The Validity of the “Diradical” Hypothesis: Direct Femtosecond Studies of the Transition-State Structures. *Science* **1994**, *266* (5189), 1359–1364.
- (32) Zewail, A. H. The Birth of Molecules. *Sci. Am.* **1990**, *263* (6), 76–83.
- (33) Fogler, H. S. Reaction Mechanisms, Pathways, Bioreactions, and Bioreactors. In *Essentials of Chemical Reaction Engineering*, 2nd ed.; Prentice Hall, 2011; pp 349–418.
- (34) Atkins, P. W.; De Paula, J. Reaction Mechanisms. In *Physical Chemistry: Thermodynamics, Structure, and Change*, 10<sup>th</sup> ed.; W.H. Freeman and Company, 2014; pp 842–848.
- (35) Hinshelwood, C. N. On the Theory of Unimolecular Reactions. *Proc. R. Soc. London, Ser. A* **1926**, *113* (763), 230–233.
- (36) Muller, P. Glossary of Terms Used in Physical Organic Chemistry (IUPAC Recommendations 1994). *Pure Appl. Chem.* **1994**, *66* (5), 1077–1184.
- (37) Qu, D. R.; Zheng, Y. G.; Jing, H. M.; Yao, Z. M.; Ke, W. High Temperature Naphthenic Acid Corrosion and Sulphidic Corrosion of Q235 and 5Cr1/2Mo Steels in Synthetic Refining Media. *Corros. Sci.* **2006**, *48* (8), 1960–1985.
- (38) Jin, P.; Robbins, W.; Bota, G. Mechanism of Magnetite Formation in High Temperature Corrosion by Model Naphthenic Acids. *Corros. Sci.* **2016**, *111*, 822–834.
- (39) Jin, P.; Nestic, S. Mechanism of Magnetite Formation in High Temperature Naphthenic Acid Corrosion by Crude Oil Fractions. *Corros. Sci.* **2017**, *115*, 93–105.
- (40) Jin, P.; Bota, G.; Robbins, W.; Nestic, S. Analysis of Oxide Scales Formed in the Naphthenic Acid Corrosion of Carbon Steel. *Energy Fuels* **2016**, *30* (8), 6853–6862.
- (41) Pestman, R.; Koster, R. M.; Pieterse, J. A. Z.; Ponec, V. Reactions of Carboxylic Acids on Oxides. *J. Catal.* **1997**, *168* (2), 255–264.
- (42) Yakerson, V. I. Mechanism of Thermal Decomposition of Salts of Carboxylic Acids. *Bull. Acad. Sci. USSR, Div. Chem. Sci. (Engl. Transl.)* **1963**, *12* (6), 914–921.
- (43) Yu, W. W.; Falkner, J. C.; Yavuz, C. T.; Colvin, V. L. Synthesis of Monodisperse Iron Oxide Nanocrystals by Thermal Decomposition of Iron Carboxylate Salts. *Chem. Commun. (Cambridge, U. K.)* **2004**, *20*, 2306–2307.
- (44) Bronstein, L. M.; Atkinson, J. E.; Malyutin, A. G.; Kidwai, F.; Stein, B. D.; Morgan, D. G.; Perry, J. M.; Karty, J. A. Nanoparticles by Decomposition of Long Chain Iron Carboxylates: From Spheres to Stars and Cubes. *Langmuir* **2011**, *27* (6), 3044–3050.
- (45) Kwon, S. G.; Piao, Y.; Park, J.; Angappane, S.; Jo, Y.; Hwang, N.-M.; Park, J.-G.; Hyeon, T. Kinetics of Monodisperse Iron Oxide

Nanocrystal Formation by “Heating-Up” Process. *J. Am. Chem. Soc.* **2007**, *129* (41), 12571–12584.

(46) Lassenberger, A.; Grünewald, T. A.; van Oostrum, P. D. J.; Rennhofer, H.; Amenitsch, H.; Zirbs, R.; Lichtenegger, H. C.; Reimhult, E. Monodisperse Iron Oxide Nanoparticles by Thermal Decomposition: Elucidating Particle Formation by Second-Resolved in Situ Small-Angle X-Ray Scattering. *Chem. Mater.* **2017**, *29* (10), 4511–4522.

(47) Heineken, F. G.; Tsuchiya, H. M.; Aris, R. On the Mathematical Status of the Pseudo-Steady State Hypothesis of Biochemical Kinetics. *Math. Biosci.* **1967**, *1* (1), 95–113.

(48) Patel, I.; Bota, G.; Young, D. Evaluation of Reactive Sulfur for Improved Corrosion Predictions in Oil Refineries. In *AMPP Annual Conference + Expo 2022, Proceedings of Oil Refining Industry Corrosion Symposium*, San Antonio, Texas, 2022; D031S030R003.

(49) Bota, G. M. *Corrosion of Steel at High Temperature in Naphthenic Acid and Sulfur Containing Crude Oil Fractions*. Ph.D. Dissertation, Ohio University: Athens, OH, 2010. [http://rave.ohiolink.edu/etdc/view?acc\\_num=ohiou1289941947](http://rave.ohiolink.edu/etdc/view?acc_num=ohiou1289941947).

(50) Bota, G.; Kurapati, Y.; Jin, P.; Robbins, W. Sulfur/TAN Ratio Effect on Iron Sulfide (FeS) Scale Properties Challenged in Continuous Oil Flow. In *CORROSION 2019, Proceedings of Refining Industry Corrosion Symposium*, NACE International, Publications Division: Nashville, Tennessee, USA, 2019, C2019–13490.

(51) Bota, G. M.; Qu, D.; Nescic, S.; Wolf, H. A. Naphthenic Acid Corrosion of Mild Steel in the Presence of Sulfide Scales Formed in Crude Oil Fractions at High Temperature. In *CORROSION 2010*, NACE International, Publications Division: San Antonio, Texas, 2010; 10353.

(52) Yépez, O. Influence of Different Sulfur Compounds on Corrosion Due to Naphthenic Acid. *Fuel* **2005**, *84* (1), 97–104.

(53) Jin, P.; Robbins, W.; Bota, G. High-Temperature Corrosion by Carboxylic Acids and Sulfidation under Refinery Conditions—Mechanism, Model, and Simulation. *Ind. Eng. Chem. Res.* **2018**, *57* (12), 4329–4339.

(54) Tebbal, S. Critical Review of Naphthenic Acid Corrosion. In *CORROSION 99*, NACE International, Publications Division: San Antonio, Texas, 1999; NACE-99380.

(55) Mandal, P. C.; Nagarajan, T. Kinetics and Reaction Pathways of Total Acid Number Reduction of Cyclopentane Carboxylic Acid Using Subcritical Methanol. *Polym. J. Chem. Technol.* **2016**, *18* (3), 44–49.

(56) Davis, R.; Schultz, H. P. Studies of Thermal Decarboxylation of Iron Carboxylates. I. Preparation of Symmetrical Aliphatic Ketones<sup>1,2</sup>. *J. Org. Chem.* **1962**, *27* (3), 854–857.

(57) Patrick, B. N.; Chakravarti, R.; Devine, T. M. Dynamic Measurements of Corrosion Rates at High Temperatures in High Electrical Resistivity Media. *Corros. Sci.* **2015**, *94*, 99–103.

(58) Patel, I.; Bota, G.; Young, D. Mechanistic Insights into Refinery Sulfidation Corrosion. In *AMPP Annual Conference + Expo 2023, Proceedings of Refining Industry Corrosion Symposium*, Denver, Colorado, 2023; AMPP-2023.

(59) Jin, P.; Robbins, W.; Bota, G. Effect of Temperature on Scale Formation in High-Temperature Corrosion by Model Naphthenic Acids and Sulfur Compounds under Replenishing Conditions. *Energy Fuels* **2017**, *31* (9), 10222–10232.

(60) Hau, J. L.; Yépez, O. J.; Torres, L. H.; Vera, J. R. Measuring Naphthenic Acid Corrosion Potential with the Fe Powder Test. *Rev. Metal. (Madrid, Spain)* **2003**, *39* (Extra), 116–123.

(61) Gates-Rector, S.; Blanton, T. The Powder Diffraction File: A Quality Materials Characterization Database. *Powder Diffraction* **2019**, *34* (4), 352–360.